Journal of Nanotechnology

WILEY

RESEARCH ARTICLE OPEN ACCESS

Green Synthesized Ag–Cu/Carbon Quantum Dots as Synergistic Peroxidase-Mimicking Nanoenzymes for Colorimetric Glucose Detection

Le Thi Thanh Nhi[1,2] | Ly Diem Hang[3] | Le Thi Hoa[4] | Trinh Ngoc Dat[5] | Nguyen Van Son Lam[6] | Quach Huu Trung[6] | Phan Xuan Thuong[7] | Le Huy Thai[8] | Le Hoang Sinh[8] | Dinh Quang Khieu[4]

[1]Center for Advanced Chemistry, Institute of Research and Development, Duy Tan University, Da Nang, Vietnam | [2]Faculty of Natural Sciences, Duy Tan University, Da Nang, Vietnam | [3]College of Medicine and Pharmacy, Duy Tan University, Da Nang, Vietnam | [4]University of Sciences, Hue University, Hue City, Vietnam | [5]University of Science and Education, The University of Danang, Da Nang, Vietnam | [6]Hospital 199, Da Nang, Vietnam | [7]School of Medicine and Pharmacy, The University of Danang, Da Nang, Vietnam | [8]VN-UK Institute for Research and Executive Education, The University of Danang, Da Nang, Vietnam

Correspondence: Le Hoang Sinh (sinh.le@vnuk.udn.vn) | Dinh Quang Khieu (dqkhieu@hueuni.edu.vn)

Received: 29 July 2025 | **Revised:** 16 April 2026 | **Accepted:** 20 July 2026

Academic Editor: Munmun Bardhan

Keyword: carbon quantum dots | copper nanoparticle | glucose | green synthesis | nanozyme | peroxidase | silver nanoparticle

ABSTRACT

Peroxidase-mimicking Ag–Cu/CQDs nanocomposites were successfully synthesized *via* a green approach, in which CQDs acted as both reducing and stabilizing agents for the simultaneous formation of AgNPs and CuNPs. The resulting nanozyme system exhibited a synergistic catalytic effect, arising from enhanced electronic interactions between Ag and Cu by CQDs, thereby increasing peroxidase-like activity. This activity of Ag–Cu/CQDs was demonstrated through the catalytic oxidation of colorless 3,3′,5,5′-tetramethylbenzidine (TMB) substrate to blue TMB_{ox} via the generation of hydroxyl radicals ($OH^{\bullet}$) in the presence of H_2O_2. Based on this principle, a colorimetric glucose (GL) detection method was developed by coupling glucose oxidase (GOx) with Ag–Cu/CQDs as nanozyme catalysts. The reaction mechanism consists of two main steps: (i) the oxidation of GL by GOx generates H_2O_2, and (ii) Ag–Cu/CQDs catalyze the decomposition of H_2O_2, generating $OH^{\bullet}$, and then oxidize TMB to blue TMB_{ox}. The established system exhibited excellent catalytic performance for detecting H_2O_2 and GL, achieving detection limits of 0.14 and 0.06 mM, respectively, which are lower than those reported for some nanozyme-based GL sensors. Furthermore, the developed assay successfully analyzed human urine samples, yielding recoveries ranging from 100.0% to 104.3%. Compared with natural peroxidase enzymes, Ag–Cu/CQDs have significant advantages, including simple synthesis, high stability, and cost-effectiveness, making them promising candidates for biosensor applications.

1 | Introduction

Diabetes is a rapidly growing global health problem. According to the World Health Organization (WHO), the number of people with the disease reached approximately 451 million in 2017 and is expected to reach 693 million by 2045 [1]. The disease is characterized by hyperglycemia, which causes many serious complications related to the cardiovascular system, nervous system, eyes, and kidneys [2]. One of the critical indicators for assessing diabetes is the presence of glucose (GL) in urine. Therefore, early detection of elevated GL levels plays a vital role in diagnosing and monitoring patients' health. Currently, many methods have been developed to determine GL concentration in

the laboratory, including colorimetric [3], fluorescence [4], chemiluminescence [5], and electrochemistry [6]. Among them, the glucose oxidase (GOx)-peroxidase-based colorimetric assay is widely used due to its advantages of fast reaction time, high sensitivity, and low detection limit [7]. Colorimetric GL detection commonly relies on the enzymatic oxidation of GL by GOx to generate H_2O_2, which subsequently oxidizes 3,3′,5,5′-tetramethylbenzidine (TMB) to a blue-colored product (TMB_{ox}), enabling GL quantification via changes in color intensity [8]. Natural catalysts such as horseradish peroxidase (HRP) are commonly used to achieve highly sensitive determinations, but the synthesis and application of these enzymes are limited by their high cost, poor stability, and complicated manufacturing processes [9, 10]. Therefore, recent studies have focused on developing alternative artificial catalysts, mainly inorganic nanoparticles, that mimic the activity of peroxidase enzymes. Notably, Fe_3O_4 nanoparticles are considered one of the first nanozymes to exhibit peroxidase-like activity, opening up avenues for the development of biosensors based on inorganic nanomaterials [11]. After the advent of Fe_3O_4 nanozyme, many other nanomaterials have also been discovered to have peroxidase-like activity with the advantages of low cost, ease of fabrication, and higher stability compared to natural peroxidase enzymes. These materials include gold nanoparticles (AuNPs) [12], $ZnFe_2O_4$ nanoparticles [13], CuO nanoparticles [14], and Co_3O_4 nanoparticles [15], all of which have been widely applied in biosensors and environmental sensors [16, 17]. Ag- and Cu-based nanozymes have attracted significant interest in the development of GL colorimetric sensors, with many material systems reported to exhibit high catalytic performance, such as C-dots/AgNPs [18], $Ag@Ag_2WO_4$ NRs [19], Carbon/Silver Core/Shell Nanodots [20], Au@Ag Heterogeneous Nanorods [21], Au/Cu_2O Particles [22], Cu@Au(Ag)/Pt nanocomposite [23] which have the good catalytic ability in the colorimetric detection of GL with high sensitivity. However, existing Ag- or Cu-based nanozymes still have significant limitations, including low stability, complex synthesis processes, and especially the inability to effectively exploit the synergistic electron interactions between the catalytic components, as well as the lack of supporting materials to promote electron transport. To address these issues, the use of plant extracts for green synthesis of metal nanoparticles is gaining increasing attention due to their environmental friendliness and high efficiency. For example, Ag–Au nanoparticles have been synthesized in aqueous media using C-terminal tryptophan radicals as bioreductants, where Au^{3+} and Ag^{+} ions are reduced to metallic Au^0 and Ag^0 and subsequently nucleate into Ag–Au nanostructures [24]. Simultaneously, the reducing agents act as stabilizers, inhibiting nanoparticle aggregation and promoting uniform size distribution and stability within the solution. In recent years, carbon quantum dots (CQDs) derived from biomass, a type of nanoscale material characterized by spherical morphology and sizes below 10 nm, have been extensively utilized in the green synthesis of metal nanomaterials [25, 26]. The synthesis of CQDs proceeds through a carbonization process, in which the biomass precursors are decomposed, transforming them into carbon-based structures. Notably, the obtained CQDs retain the active functional groups from the original biomass, providing a favorable surface for further functionalization [27]. Besides acting as reducing agents and stabilizers in the formation of metal nanoparticles, CQDs also enhance catalytic performance due to their large surface area, good conductivity, and the presence of multiple active functional groups such as hydroxyl (-OH), carboxyl (-COOH), and amino (-NH_2) [28]. These properties have been demonstrated through recent studies, showing the outstanding potential of CQDs in catalytic and biosensor applications [29, 30].

Previous studies on colorimetric nanozymes for GL detection mainly focused on single metal or metal oxide material systems, which limit their catalytic efficiency. At the same time, the synergistic catalytic effect between Ag–Cu bimetallic nanoparticles and CQDs-in which Ag and Cu can mutually enhance the electron donor-acceptor ability, and CQDs act as reductants, stabilizers, and electron transfer mediators-has not been systematically studied. In this study, a green, simple, and efficient approach was applied to develop Ag–Cu/CQDs materials with peroxidase catalytic activity for the colorimetric detection of GL in urine. Although blood GL monitoring remains widely used, urine GL analysis offers an easy and noninvasive continuous monitoring solution. High urinary GL concentrations are strongly associated with hyperglycemia and renal GL excretion thresholds, making urine a clinically significant substrate for evaluating GL-related metabolic disorders [31]. CQDs were synthesized from turmeric starch (TS) using the hydrothermal method, acting as reducing and stabilizing agents, helping immobilize AgNPs and CuNPs, preventing agglomeration, and promoting the synergistic effect among the components of the material. Ag–Cu/CQDs materials have many outstanding advantages, such as a green synthesis process, low cost, easy implementation, nonpolluting, and high stability, as well as good biocompatibility, thanks to the presence of functional groups from biomass precursors [31, 32]. The peroxidase-like activity of Ag–Cu/CQDs was evaluated and subsequently applied for colorimetric GL detection in urine. The research results showed that Ag–Cu/CQDs are a potential material that can replace peroxidase enzymes in biochemical detection and biomedical diagnostic applications.

2 | Material

2.1 | Chemicals

TS used to synthesize CQDs was purchased from Hue, Vietnam. The chemicals used in the experiments, including $AgNO_3$, $Cu(NO_3)_2.3H_2O$, GOx, H_2O_2, TMB, NaOH, and HCl, were obtained from Sigma-Aldrich (USA). GL, lactose, fructose, L-cysteine, CH_3COOH, CH_3COONa, NaH_2PO_4, and Na_2HPO_4 were purchased from Sinopharm Chemical Reagent Co., Ltd (China). Deionized water (DIW) was used for all experiments.

2.1.1 | Synthesis of CQDs From TS

CQDs from TS were synthesized hydrothermally by mixing 0.04 g TS in 50 mL distilled water at 180°C for 16 h. After cooling to room temperature, the resulting solution was centrifuged at 4500 rpm for 10 min to remove insoluble carbon residues. The clear, pale-yellow solution containing CQDs was recovered and used directly for further experiments without purification. From published research [33], this process yielded almost complete conversion efficiency, with a residual amount of approximately 0.8% (w/w) and a CQD concentration of approximately 0.8 mg/mL; therefore, CQDs were used based on the solution volume, as described in the same methodology.

2.1.2 | Synthesis of Ag–Cu/CQDs

CQDs-based silver–copper nanoparticles (Ag–Cu/CQDs) were synthesized through the co-reduction of $AgNO_3$ and $Cu(NO_3)_2$ precursors in the presence of CQDs. CQDs acted as both a reducing and stabilizing agent, reducing Ag^+ and Cu^{2+} to metal nanoparticles, AgNPs and CuNPs, respectively, while limiting the agglomeration phenomenon. Specifically, 20 mL of 2 M $AgNO_3$ solution and 20 mL of 2 M $Cu(NO_3)_2$ solution were mixed into 10 mL of CQDs solution and then stirred on a magnetic stirrer heated at 80°C. During this process, the pH of the mixture was adjusted to 11 using 0.5 M NaOH, resulting in a final reaction volume of approximately 60 mL. Next, the mixture was boiled for 10 min and then cooled to room temperature. The result was a reddish-brown solution, representing the formation of stable nanosized Ag–Cu/CQDs. In addition, the individual synthesis of Ag/CQDs and Cu/CQDs components was also carried out following the same procedure but without the presence of the other metal precursor, helping to identify the role of each component in the composite material system (Scheme 1).

2.2 | Characterization of Materials

The prepared materials were thoroughly characterized using advanced techniques, including transmission electron microscopy (TEM), scanning electron microscopy (SEM) coupled with energy-dispersive X-ray spectroscopy (EDX), Fourier-transform infrared spectroscopy (FT-IR), and X-ray diffraction (XRD), to study their size, surface morphology, elemental composition, functional groups, and crystalline structure. UV–visible spectrophotometry (UV–Vis) was used to measure the absorbance of samples at 652 nm.

2.3 | Peroxidase Activity of Ag–Cu/CQDs

The peroxidase-like activity of the Ag–Cu/CQDs materials was evaluated by catalyzing the oxidation of colorless TMB into its blue oxidized form (TMB_{ox}). In a typical procedure, 300 μL of 400 mg/L H_2O_2, 200 μL of 5 mM TMB, and 0.545 g/L of catalyst were mixed in 5 mL of acetate buffer (pH 4), prepared from 0.2 M CH_3COOH and 0.2 M CH_3COONa. The mixture was incubated at 30°C for 40 min, after which the absorbance was measured at 652 nm using a UV–Vis spectrophotometer. Furthermore, key experimental parameters (pH, catalyst concentration, reaction time, and H_2O_2 concentration) were systematically optimized. To ensure a stable pH throughout the reaction, all experiments were performed in acetate buffer (pH 4.0) rather than adjusting the pH directly with acid or base.

2.4 | H_2O_2 and GL Colorimetric Detection by Ag–Cu/CQDs

For the detection of H_2O_2, different concentrations of H_2O_2 were added to the reaction mixture and incubated at 30°C for 40 min under the optimized conditions in Section 2.3. Then, the spectrophotometric measurements were performed at 652 nm. In the case of GL quantification via the colorimetric method, GL solutions with different concentrations ranging from 0 to 4.0 mM were first reacted with O_2 in the presence of 100 μL GOx, and 500 μL pH 7 buffer, and the process was incubated for 30 min. Then, 0.545 g/L Ag–Cu/CQDs, 200 μL 5 mM TMB, and 5 mL pH 4 buffer were added to the reaction mixture, respectively. Then, the reaction system was incubated for 40 minutes at 30°C. The resulting mixture was analyzed, and the absorbance signal was recorded at 652 nm using a UV–Vis spectrophotometer. All measurements were conducted in independent triplicates ($n = 3$). The linear range was determined from the calibration curve ($y = ax + b$) by linear regression. The limit of detection (LOD) and limit of quantification (LOQ) were calculated as 3 and $10\sigma/S$, respectively, where σ is the standard deviation of blank measurements and S is the slope of the calibration curve [34]. This statistical treatment ensures that the analytical results are robust and reproducible.

2.5 | Real Sample Analysis

The analysis of GL in real samples using Ag–Cu/CQDs by colorimetric mechanism will be performed by adding GL standard at 03 different concentrations to the urine sample matrix. Immediately after collection, urine samples of healthy people are diluted 150 times with distilled water and the GL standard. The process of detecting GL in urine will be performed as in Section 2.4, and the absorption intensity signal at 652 nm wavelength will be recorded by a UV–Vis spectrophotometer.

3 | Results and Discussion

3.1 | Characterization

Figure 1 shows the TEM and SEM images of Ag/CQDs, Cu/CQDs, and Ag–Cu/CQDs at different magnifications to observe the prepared materials' morphology. The results showed that the composites had no hollow spherical structure, and the nanoparticles were relatively uniformly distributed. Specifically, the AgNPs were spherical in shape, while the CuNPs existed in the form of thin sheets. Both morphologies were present in the Ag–Cu/CQDs composite samples, with the mean particle size at 52.4 nm (±14.3 nm). The particle sizes of the AgNPs ranged from 10 to 35 nm, with an average diameter of about 20.4 nm. Meanwhile, the CuNPs had a sheet-like structure with an average length of about 102.2 nm. The almost complete transparency of the nanosheets indicated that they had an ultrathin structure, and the presence of numerous nanodots on the surface of the nanosheets demonstrated that the CQDs were effectively attached to the AgNPs and CuNPs, contributing to the formation of a homogeneous nanomaterial. Furthermore, the EDX elemental map in Figure 1i clearly shows the significant elements, including C, O, Ag, and Cu, distributed in Ag–Cu/CQDs. The result is strong evidence that we have successfully synthesized nanostructured Ag–Cu/CQDs materials.

In addition to TEM, SEM, and EDX techniques, XRD and FT-IR techniques were also used to determine the structural and chemical characteristics of the synthesized materials, contributing to the confirmation of the formation of crystalline phases and the chemical bonds in the material system. Figure 2a shows the XRD diffraction patterns of the Ag/CQDs, Cu/CQDs, and Ag–Cu/CQDs samples. Among them, the characteristic peaks of Ag observed at 38.1°, 64.3°, and 79.4°, corresponding to the (111), (220), and (311) crystal planes, respectively, consistent with the JCPDS No. 003-0921 database [35], were visible on the Ag/CQDs and Ag–Cu/CQDs samples. In addition, the diffraction peak at 43.8° corresponding to the (111) plane of Cu, consistent with the JCPDS No. 04-0836 data [35, 36] was also detected on the Cu-containing samples. These sharp diffraction peaks confirm the

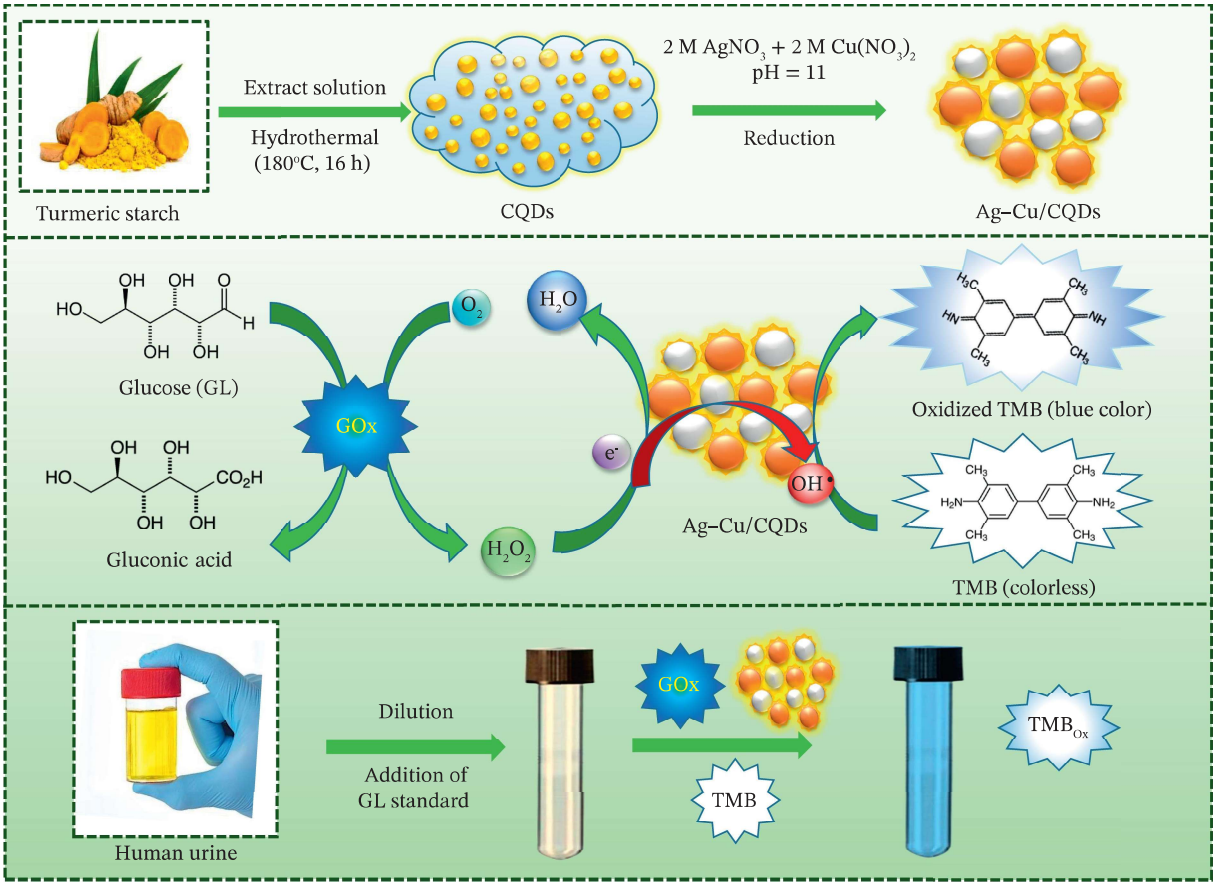

SCHEME 1 | The illustration of Ag–Cu/CODs synthesis and GL detection.

presence of highly crystalline Ag and Cu nanoparticles in the composites. In the FTIR spectrum of Ag–Cu/CQDs, weak absorption bands observed at 597.4 and 775.8 cm^{-1} can be tentatively associated with Cu-O-related vibrations [37], while the band at ~510 cm^{-1} may be attributed to Ag-O vibrations [38]. Similar characteristics were also observed in Cu/CQDs and Ag/CQDs, respectively, suggesting the presence of metal-oxygen interactions on the CQD surface. In addition, the low-intensity peaks at 3470 and 2969 cm^{-1} indicated the presence of the -OH group and C-H [38–40], and the peak at 1115 cm^{-1} was attributed to the characteristic vibration of the C-O-C group, which is a characteristic functional group on the surface of CQDs synthesized by the green method from TS. During the reduction of metal ions to form AgNPs and CuNPs, the hydroxyl and carboxyl groups on CQDs act as reducing agents and surface ligands [41, 42]. The stable presence of characteristic peaks of CQDs in the FTIR spectra of the synthesized materials suggests that CQDs are not only material matrices but also play an essential role in stabilizing and dispersing metal nanoparticles (AgNPs, CuNPs) through surface interactions.

3.2 | Peroxidase Activity of Ag–Cu/CQDs

The peroxidase-like activity of the Ag–Cu/NPs catalyst was evaluated by oxidizing TMB in the presence of H_2O_2 at 30°C. Figure 3a shows the absorbance of different reaction systems in the wavelength range of 500–800 nm, based on the color change of TMB from colorless to a characteristic blue at 652 nm [43] in the presence of H_2O_2 and the catalyst. Specifically, the reaction system consisting of only TMB and H_2O_2 (without Ag–Cu/NPs) showed no significant color change. At the same time, the absorption signal increased sharply in the presence of the Ag–Cu/NPs catalyst, demonstrating that Ag–Cu/NPs have peroxidase-like enzyme activity when catalyzing the reaction between TMB and H_2O_2 [15]. Moreover, the absorbance signal at 652 nm was notably low in the reaction system containing only TMB and Ag–Cu/NPs (without H_2O_2), indicating that the catalytic process relies on dissolved oxygen in the solution. Under anaerobic conditions, the generation of reactive oxygen species from O_2 is markedly suppressed, significantly reducing catalytic activity [44]. In addition, the blue shift in the Ag/CQDs and Cu/CQDs systems was shown by the higher absorbance at 652 nm than that of the noncatalyst system and lower than that of the Ag–Cu/CQDs composite system, indicating that Ag/CQDs and Cu/CQDs also exhibited peroxidase activity. Their synergy enhanced the peroxidase-like catalytic efficiency of Ag–Cu/CQDs [42, 43].

Experimental conditions, including pH of the buffer solution, reaction time, catalyst dosage, TMB concentration, and H_2O_2 concentration, were studied in detail to optimize the catalytic process. The effect of pH in the range of 3–9 on the peroxidase-like activity of Ag–Cu/CQDs was evaluated through the oxidation of TMB in the presence of H_2O_2 (Figure 3b). The results showed that Ag–Cu/CQDs had the highest catalytic efficiency at pH 4, consistent with previous studies assuming that TMB oxidation was favorable in acidic environments [42, 44]. Reaction time also significantly affected the catalytic efficiency (Figure 3c). The catalytic efficiency increased gradually as the reaction time

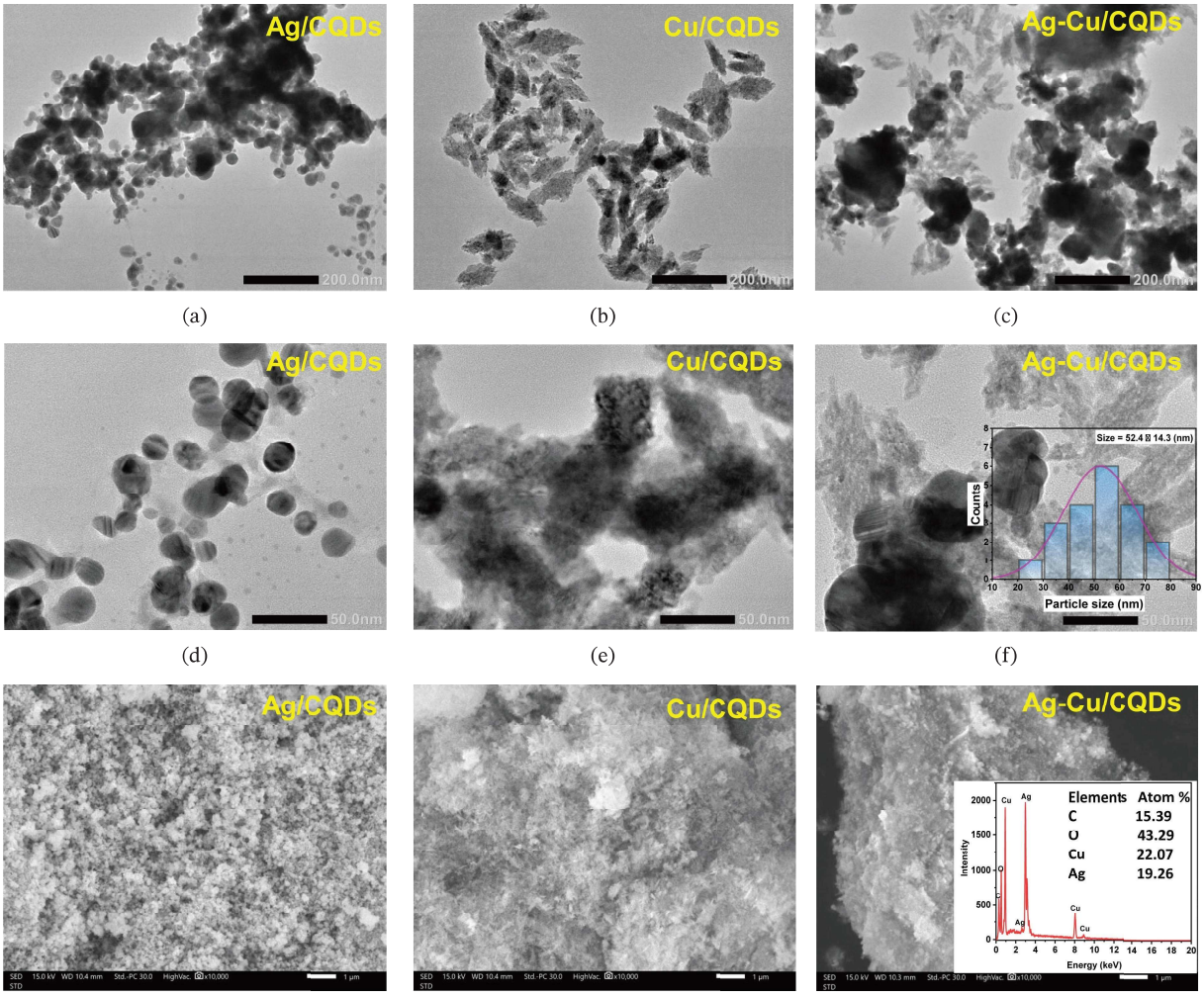

FIGURE 1 | The TEM images of Ag/CQDs (a, d); Cu/CQDs (b, e); Ag–Cu/CQDs (c, f) at different resolutions and particle size distribution histogram of Ag–Cu/CQDs (inset of f); the SEM images of Ag/CQDs (g); Cu/CQDs (h); Ag–Cu/CQDs (i) and the EDX spectrum of Ag–Cu/CQDs (inset of i).

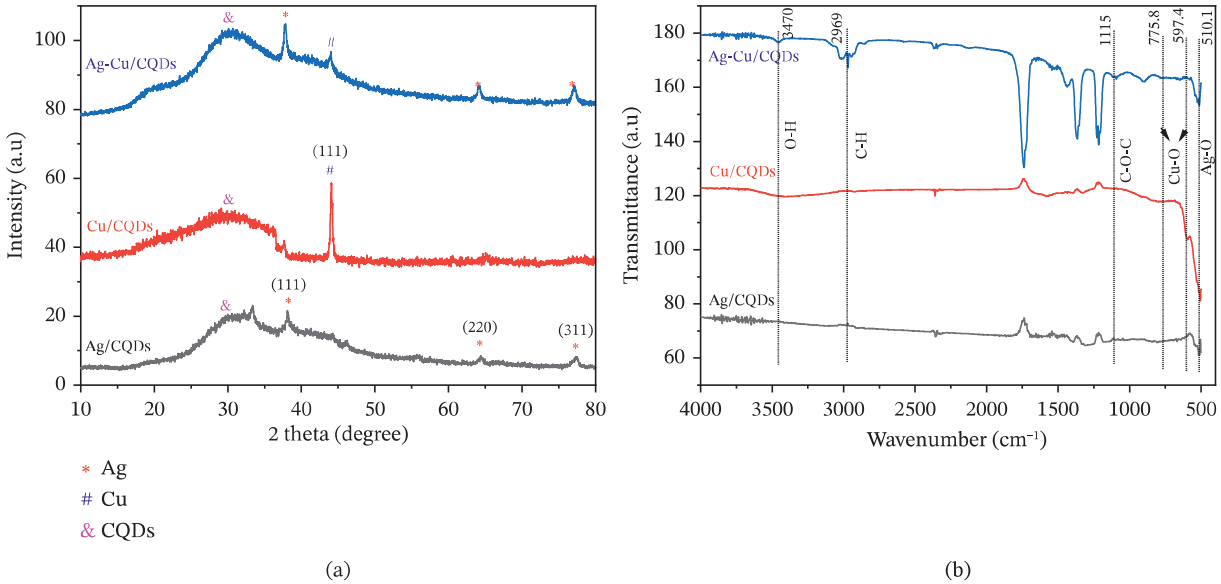

FIGURE 2 | The XRD patterns (a) and FTIR spectra (b) of Ag/CQDs, Cu/CQDs, Ag–Cu/CQDs.

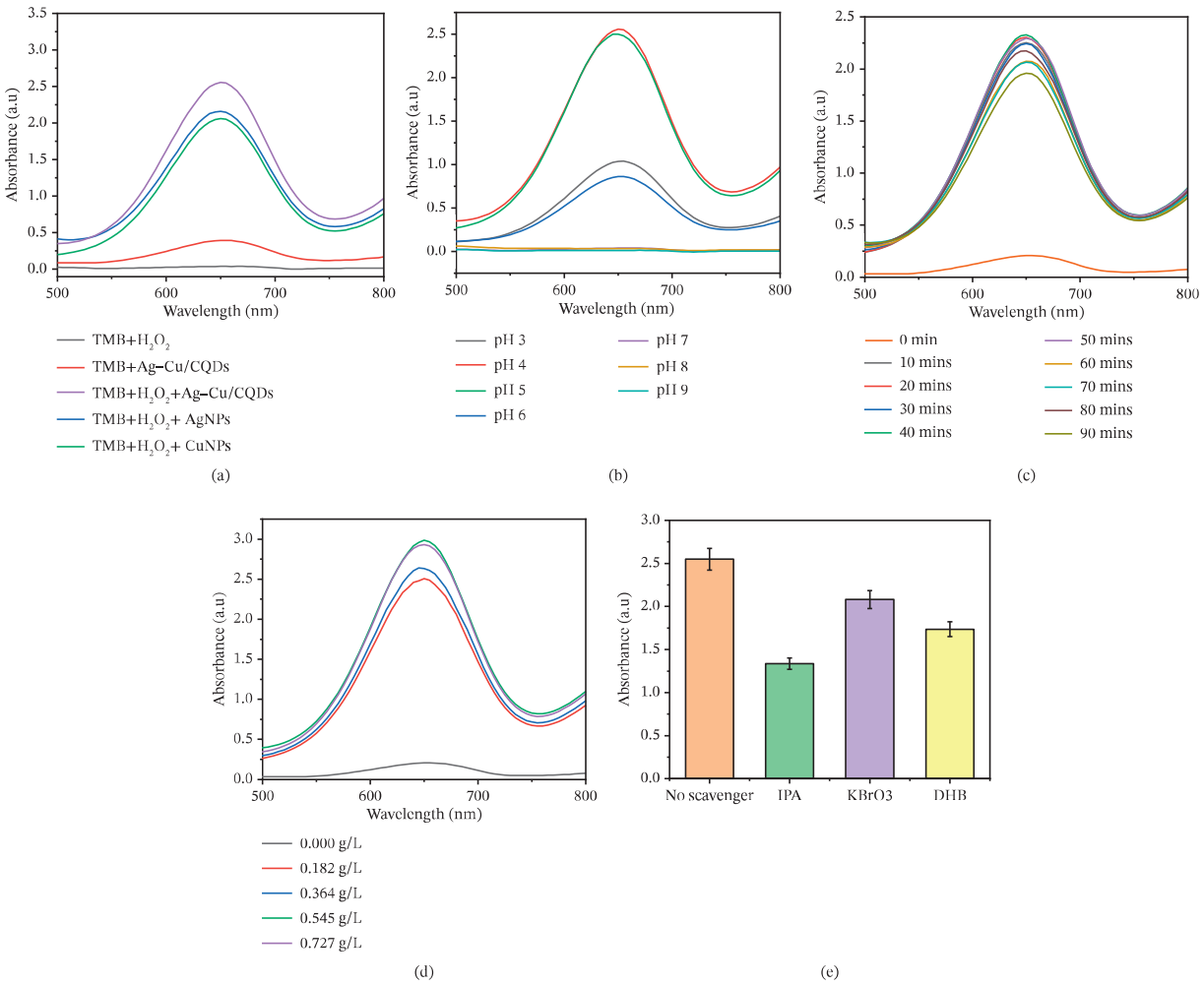

FIGURE 3 | UV-Vis spectra of the different reaction systems (a); effect of pH (b); effect of reaction time (c); dose of catalyst (d) and scavengers (e) for the oxidation of TMB by H_2O_2.

extended from 0 to 40 min because of the prolonged contact of the substrate H_2O_2 and TMB with the catalyst. Then, there was a slight decrease in the 40–90 min range, implying that the catalytic efficiency slowed down with increasing time [45]. It showed that the optimal reaction time was 40 min to achieve the highest catalytic efficiency. Based on the optimal results of pH (4.0) and reaction time (40 min), the effect of Ag–Cu/CQDs catalyst dosage was investigated at 30°C, H_2O_2 concentration 400 mg/L, and TMB concentration 5 mM. The results obtained (Figure 3d) showed that when the Ag–Cu/CQDs dosage increased from 0 to 0.545 g/L, the absorbance at 652 nm gradually increased, reflecting the increase in catalytic activity. However, the catalytic efficiency decreased slightly when the dosage continued to increase to 0.727 g/L. The reason may be that the excess catalyst hinders the contact between TMB and the active sites on the material surface, leading to a decrease in catalytic efficiency [38]. This result determined the optimal catalyst dosage to be 0.545 g/L for further experiments.

Based on the optimized conditions, the peroxidase-like catalytic activity of the material was also investigated through free radical trapping experiments using isopropyl alcohol (IPA, trapping $OH^{\bullet}$) [46], 3,4-dihydroxybenzoic acid (DHB, trapping $O_2^{\bullet -}$) [47], and $KBrO_3$ (trapping e^-) [48], to support the study of the reaction catalytic mechanism. All reactions were carried out under ambient laboratory light without intentional light irradiation. The results presented in Figure 3e show that the absorption intensity at 652 nm decreased significantly with the addition of IPA (47.6% inhibition), indicating that $OH^{\bullet}$ radicals played the most crucial role in the oxidation of TMB, as in a previous study [49]. When DHB was used, the absorption signal decreased to a moderate level (31.9%), indicating that $O_2^{\bullet -}$ was also an active agent contributing to the reaction process. The decrease in absorption upon the addition of $KBrO_3$ (18.4%) suggests that the electron transfer pathway (e^-) also participated in the catalytic activity. However, the influence was lower than that of the other two agents. Taken together, these results show that all three active species are involved in the peroxidase-like mechanism of the material, with the contribution levels in the order: $OH^{\bullet} > O_2^{\bullet -} > e^-$.

3.3 | Kinetic Studies of the Peroxidase Activity

The peroxidase-like catalytic kinetics of Ag–Cu/CQDs were investigated through steady-state kinetic parameters, based on the oxidation reaction of TMB in the presence of H_2O_2 in the proposed reaction system. The investigation was carried out by varying the concentrations of TMB and H_2O_2 over time in the

proposed reaction system, thereby evaluating the reaction rate. The obtained kinetic data were analyzed using the Michaelis–Menten equation, $V_0 = V_{max}[S]/(K_m + [S])$, where V_0 is the initial reaction rate, V_{max} is the maximum reaction rate, [S] is the substrate concentration (TMB or H_2O_2), and K_m is the Michaelis–Menten constant, representing the catalyst's affinity to the substrate [50]. The initial reaction rate v was calculated from the optical absorption data according to the Lambert–Beer law, using a molar absorption coefficient of 39,000 $M^{-1}\cdot cm^{-1}$ for the oxidation product of TMB [51].

Figure 4 presents the steady-state kinetic analysis of Ag–Cu/CQDs with respect to TMB and H_2O_2, including the nonlinear Michaelis–Menten curve (Figure 4a,c) and the corresponding double inverse Lineweaver–Burk plots (Figure 4b,d). The apparent kinetic parameters (K_m and V_{max}) were determined primarily from the nonlinear Michaelis–Menten fitting method, and compared with previously reported nanoenzymes (Table 1). K_m is an important parameter reflecting the affinity of the enzyme for the substrate. The lower the K_m value, the higher the affinity between the enzyme and the substrate, that is, the enzyme can bind to the substrate more effectively at low concentrations [55]. Compared with HRP, the Ag–Cu/CQDs nanocomposite showed a K_m value for TMB of 0.091 mM, slightly lower than that of HRP (0.434 mM) [56], indicating that Ag–Cu/CQDs have a higher affinity for TMB than the native enzyme, requiring a lower TMB concentration to achieve the maximum reaction rate. In contrast, the K_m value for H_2O_2 of Ag–Cu/CQDs was 0.013 mM, much lower than that of HRP (3.70 mM), indicating a greater affinity for the H_2O_2 substrate than the native enzyme [57]. In addition, the V_{max} of Ag–Cu/CQDs for TMB and H_2O_2 were recorded as 2.67×10^{-8} and 0.81×10^{-8} $M\cdot s^{-1}$, respectively (Table 1), indicating that the composites possess peroxidase catalytic activity. Compared with the other published materials in Table 1, these results confirm the potential application of Ag–Cu/CQDs as an efficient peroxidase-mimicking catalyst in colorimetric systems based on the TMB oxidation reaction.

3.4 | Colorimetric Detection of H_2O_2 and GL

Based on the good peroxidase catalytic ability of the Ag–Cu/CQDs material, this nanosystem catalyzes the decomposition reaction of H_2O_2, generating reactive oxygen species that can oxidize TMB from colorless form to TMB_{ox} with a characteristic blue color [58]. This process is applied to develop a sensitive and selective H_2O_2 detection method. In this experiment, H_2O_2 concentrations from 0.555 to 55.55 mM were investigated under the optimal conditions established in Section 3.2. The results presented in Figure 5a show that as the H_2O_2 concentration increases, the blue color intensity at the characteristic wavelength of 652 nm also increases correspondingly, reflecting the increasing formation of TMB_{ox}. The linear relationship between H_2O_2 concentration and absorption intensity was established with the regression equation, $y = 0.01215x + 0.6975$ ($R^2 = 0.986$) (Figure 5b). The method gave a LOD of 0.14 mM and a LOQ of 0.42 mM [59], confirming the potential application of Ag–Cu/CQDs materials in color sensor systems to detect H_2O_2, not only with high efficiency and sensitivity but also user-friendly through easily observable color changes even at low H_2O_2 concentrations.

Based on the catalytic mechanism of the enzyme GOx, GL is oxidized to gluconic acid and simultaneously produces H_2O_2 in the presence of molecular oxygen [60]. The amount of H_2O_2 produced continues to react with the substrate TMB under the catalysis of peroxidase activity, creating a characteristic blue product. This principle has been developed into a sensitive colorimetric method to detect GL. The color intensity of the TMB oxidation product is proportional to the GL concentration, allowing indirect quantification of GL through the color signal of the reaction system [19]. Under optimal conditions, the Ag–Cu/CQDs material was applied to detect GL through the experimental series described in Section 2.3, with the GL concentration ranging from 40 to 4800 μM. The results presented in Figure 5c show that the absorption intensity at 652 nm gradually increases with the GL concentration. Correlation analysis between color intensity and GL concentration showed a good linear relationship, with the regression equation $y = 0.00029x + 0.23833$ and the correlation coefficient $R^2 = 0.998$ (Figure 5d)). Based on this equation, LOD and LOQ were calculated as 0.06 and 0.18 mM, respectively. The Ag–Cu/CQDs showed good catalytic performance with a low LOD value and a wide linear range, demonstrating a sensing performance comparable to or competitive with many previously published material systems, as shown in Table 2. This exceptional performance stems from the synergistic effect between Ag and Cu nanoparticles with CQD bridges, which promotes faster electron transfer and enhanced peroxidase-like catalytic activity. Compared with single-metal nanozymes, this bimetallic-conductive structure not only provides more active sites but also significantly enhances charge separation and transfer during the reaction. These results confirm that Ag–Cu/CQDs is a promising sensing platform for GL detection, offering high sensitivity and good stability, and is promising for expanding its applications in biological systems and practical analysis.

The selectivity of Ag–Cu/CQDs materials in detecting GL by colorimetric method was verified through experiments examining the effects of interfering agents. In the experiment, the GL concentration was kept constant at 60 mM while common substrates such as fructose (30 mM), lactose (30 mM), and cysteine (30 mM) were added. The absorbance measurement results at 652 nm (Figure 6) showed that the signal intensity remained almost unchanged in the presence of these interfering agents, proving that they did not affect the GL detection efficiency of the sensor system. In particular, although cysteine is a strong reducing amino acid that can compete with TMB, the experimental results still showed no color signal degradation, consistent with previous studies [51, 55]. This can be explained by the fact that the H_2O_2 product of the GL process by GOx has a strong oxidizing power that promotes the oxidation of TMB into a stable blue product and limits the ability of cysteine to reduce TMB back, thereby ensuring the accuracy and stability of the measurement [57]. This result confirms that the Ag–Cu/CQDs material system combined with GOx has high selectivity and ensures signal stability, thanks to the preferential and specific reaction mechanism between GOx and GL, helping to minimize the impact of interference agents in the sample environment.

3.5 | Proposed Mechanism

The catalytic mechanism of the Ag–Cu/CQDs material system in the process of detecting GL through color signal is believed to originate from the ability to generate hydroxyl radicals ($^{\bullet}OH$) during the decomposition of H_2O_2 combined with effective

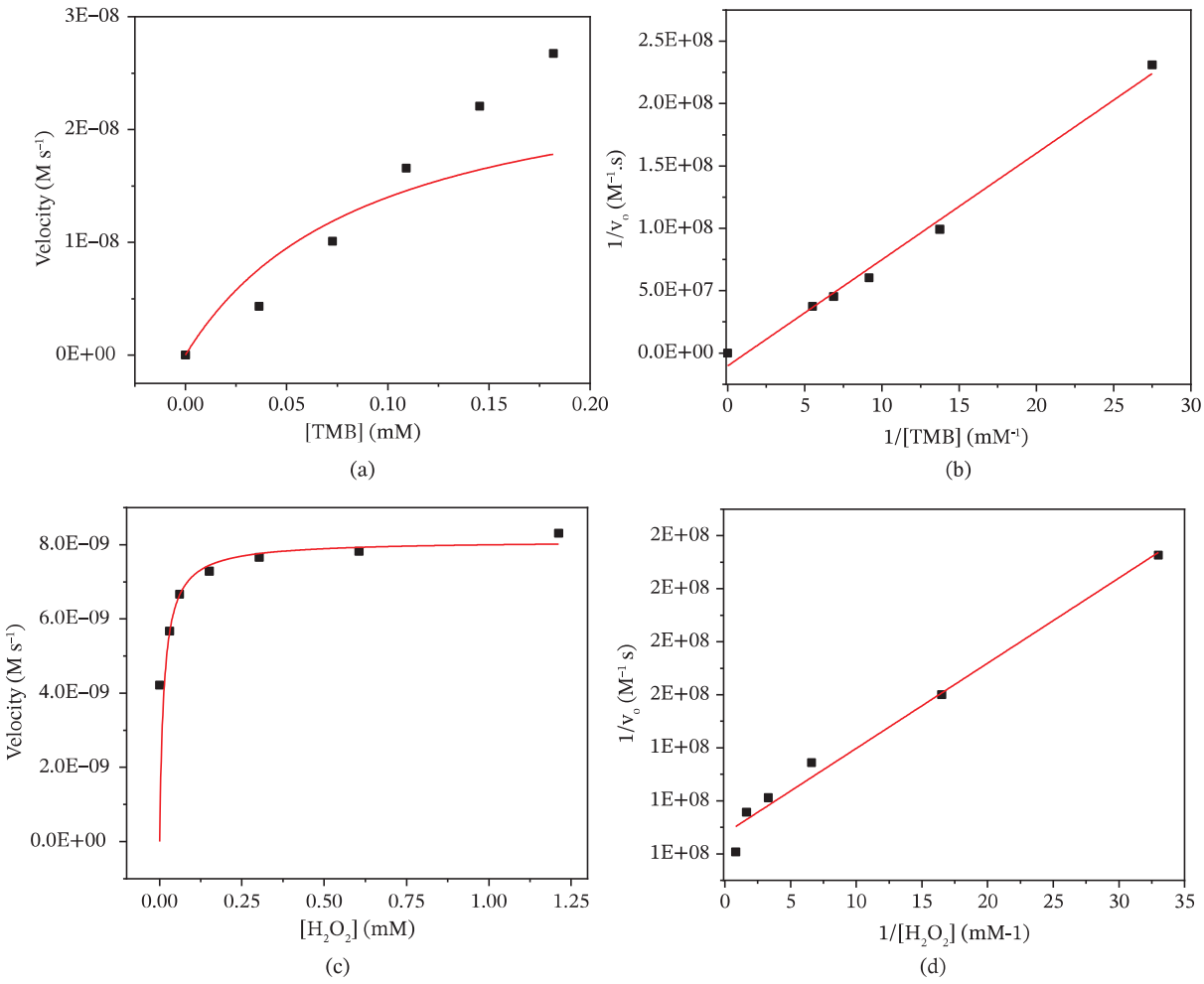

FIGURE 4 | Steady-state kinetic analysis of Ag–Cu/CQDs for TMB and H_2O_2 using nonlinear Michaelis–Menten (a, c) and Lineweaver–Burk plots (b, d).

electron transfer [47, 65]. Specifically, the GL detection process takes place in two main stages: (i) under the influence of the enzyme GOx, GL is oxidized by dissolved oxygen, producing H_2O_2 and gluconic acid [18]; (ii) the amount of H_2O_2 generated then acts as an oxidant, converting TMB from a colorless state to an oxidized form with a characteristic blue color in the presence of the Ag–Cu/CQDs catalyst. In this step, H_2O_2 is adsorbed onto the Ag–Cu/CQDs nanocomposite surface, facilitating the electron exchange between the amino groups of TMB and the material system [66]. This interaction increases the electron density and mobility in the nanocomposite network, promoting the electron transfer from Ag–Cu/CQDs to H_2O_2. As a result, H_2O_2 decomposes rapidly into water and highly active $OH^{\bullet}$ radicals. These free radicals continue to transfer electrons to TMB,

TABLE 1 | Comparison of the kinetic parameters of other catalysts.

Materials	Substances	K_m (mM)	V_{max} ($M.s^{-1}$)	Ref
Fe_3S_4	TMB	0.161	14.71×10^{-8}	[7]
	H_2O_2	0.111	13.12×10^{-8}	[7]
$ZnFe_2O_4$ MNPs	TMB	0.85	13.31×10^{-8}	[52]
	H_2O_2	1.66	7.74×10^{-8}	[52]
Co_3O_4 NPs	TMB	0.037	3.27×10^{-8}	[15]
	H_2O_2	140.07	12.10×10^{-8}	[15]
Horseradish peroxidase (HRP)	TMB	0.434	10.00×10^{-8}	[53]
	H_2O_2	3.70	8.71×10^{-8}	[53]
Fe_3O_4@Cu@Cu_2O	H_2O_2	2.3	11.00×10^{-8}	[54]
Ag–Cu/CQDs	TMB	0.091	2.67×10^{-8}	This study
	H_2O_2	0.013	0.81×10^{-8}	This study

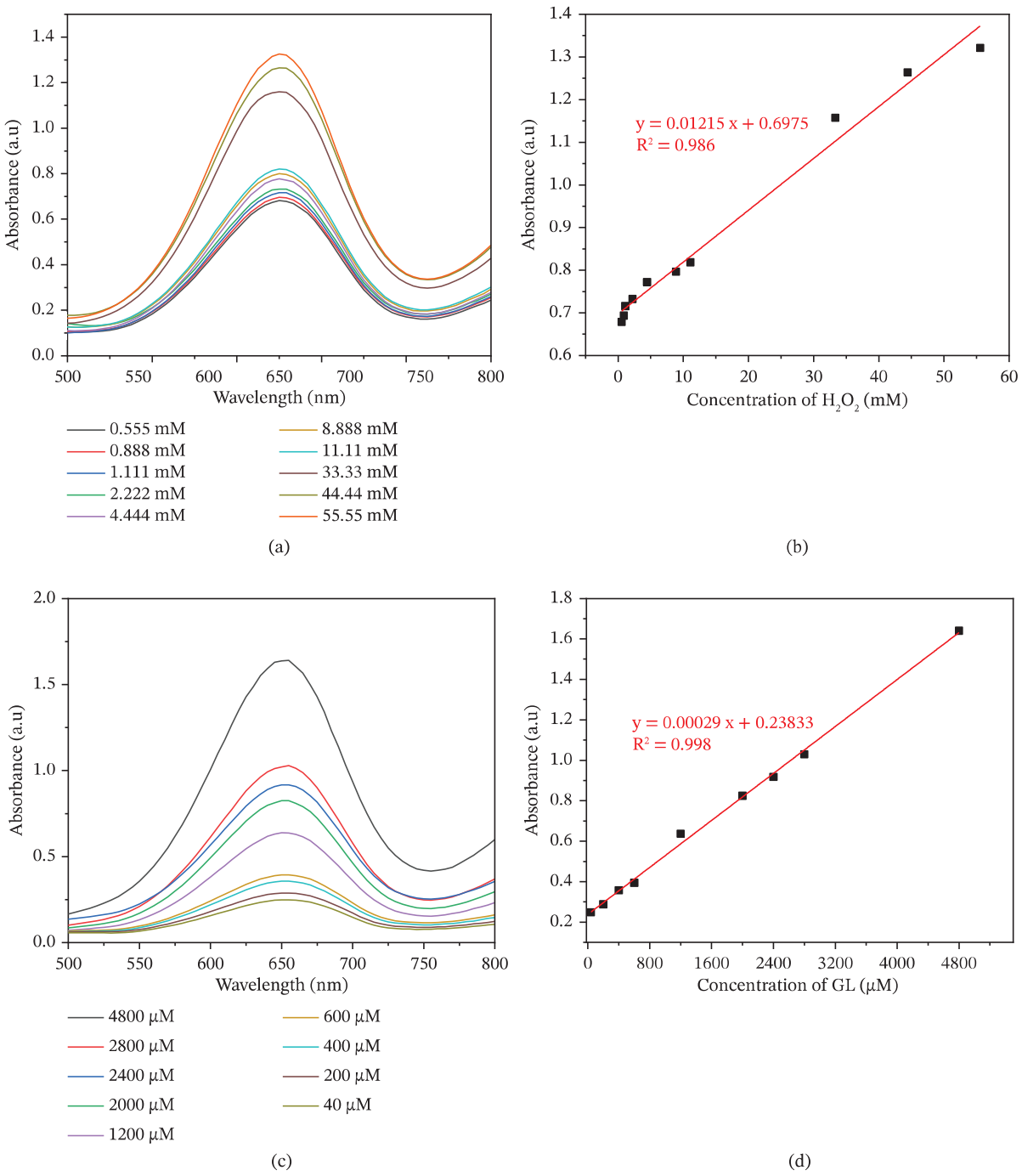

FIGURE 5 | UV–Vis spectra for oxidation of TMB at different concentrations of H_2O_2 (a); linear calibration plot of H_2O_2 (b); UV–Vis spectra for oxidation of TMB at different concentrations of GL (c); linear calibration plot of GL (d).

TABLE 2 | Comparison of linear range and LOD results of different materials for GL detection.

Materials	Analytes	Linear range (mM)	LOD (mM)	Ref
Fe_3O_4 nanoparticle	Glucose	0.05–1	0.03	[9]
Ag NPs graphene	Glucose	2–10	0.1	[61]
Au−Ag−Pt Nanoparticle	Glucose	0–10	0.289	[62]
Etching of triangular gold nanosheets (AuTNPs)	Glucose	0.2–12	0.1	[63]
CoO-OMC	Glucose	0.1–5.0	0.068	[64]
Ag–Cu/CQDs	Glucose	0.04–4.8	0.06	This study

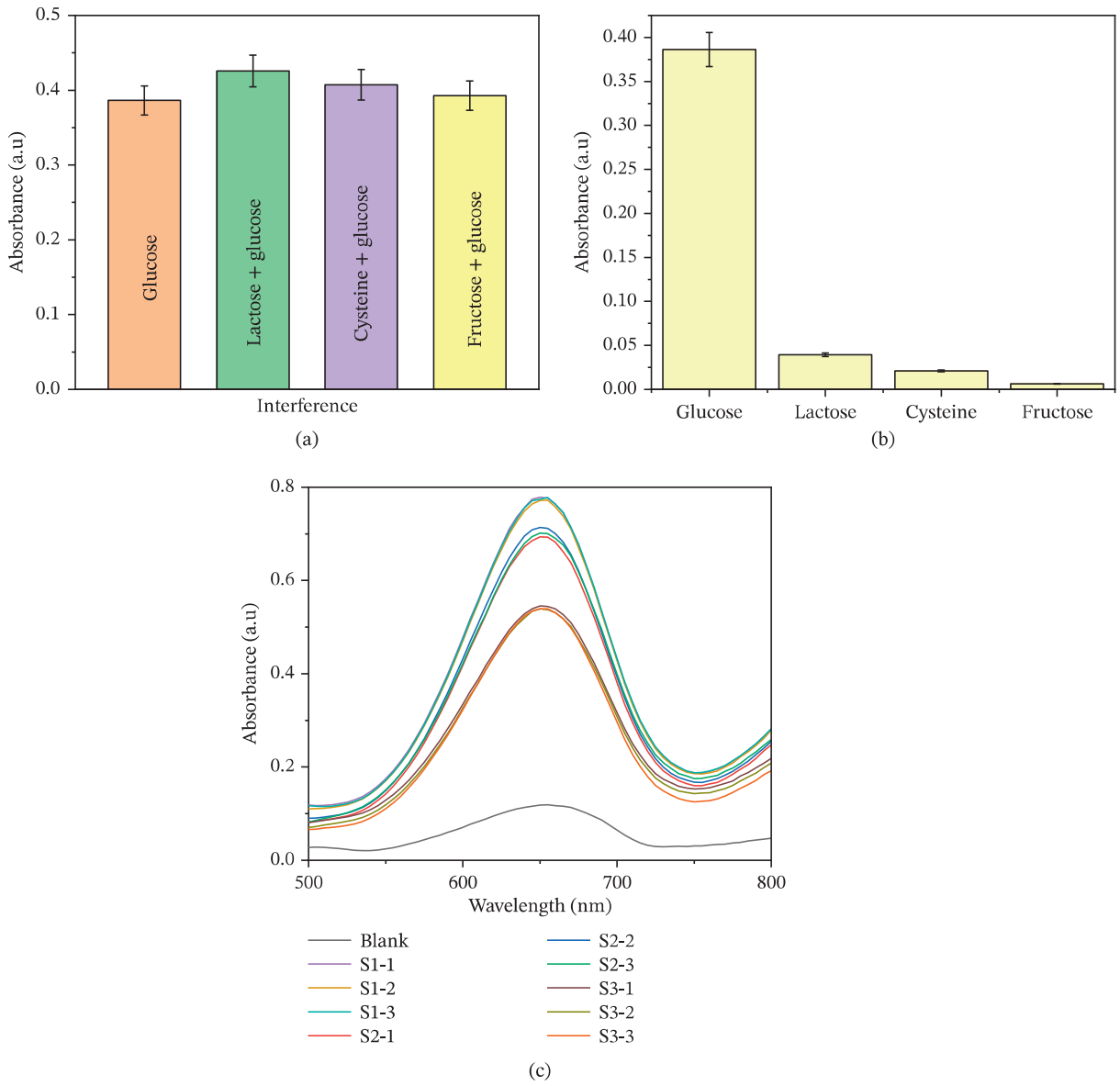

FIGURE 6 | Determination of the selectivity of GL detection (a, b); UV–Vis spectra of real sample (c) for determination of GL based on Ag–Cu/CQDs.

accelerating the oxidation of TMB into the characteristic dark blue TMB_{ox} product [67]. Notably, the presence of CQDs not only acts as effective adsorption centers, helping to fix TMB molecules onto the catalyst surface [68] but also contributes to enhancing the electron density as well as the electron transfer [69, 70] between Ag–Cu nanoparticles and the CQDs surface. In addition, according to previous research, AgNPs and CuNPs with peroxidase activity on Ag–Cu bimetallic nanomaterials exhibited improved catalytic performance due to their synergistic effect [71]. The overall mechanism of this process is illustrated in Scheme 2.

3.6 | Real Sample Analysis

The practical applicability of the proposed colorimetric method was evaluated by an experiment to detect GL in human urine samples, which was carried out using the standard addition method, similar to many previous studies [60, 66]. The urine sample was diluted 150 times with distilled water to minimize the influence of background factors without any other pretreatment steps [72]. Then, three levels of standard GL concentrations (S1, S2, and S3) were added to the sample; each level was repeated three times to check the repeatability. The reaction procedure continued as described in Section 2.5. The absorbance measurement results at 652 nm (Figure 6c) showed that the signal increased gradually, corresponding to each added GL level. Analysis of the recovery showed that the value was in the range of 100%–104.3%, and good repeatability was demonstrated through triplicate measurements at each concentration (Table 3). The negligible interference from lactose, fructose, and cysteine, together with the satisfactory recoveries in spiked urine samples, indicates that matrix effects from urine components are minimal

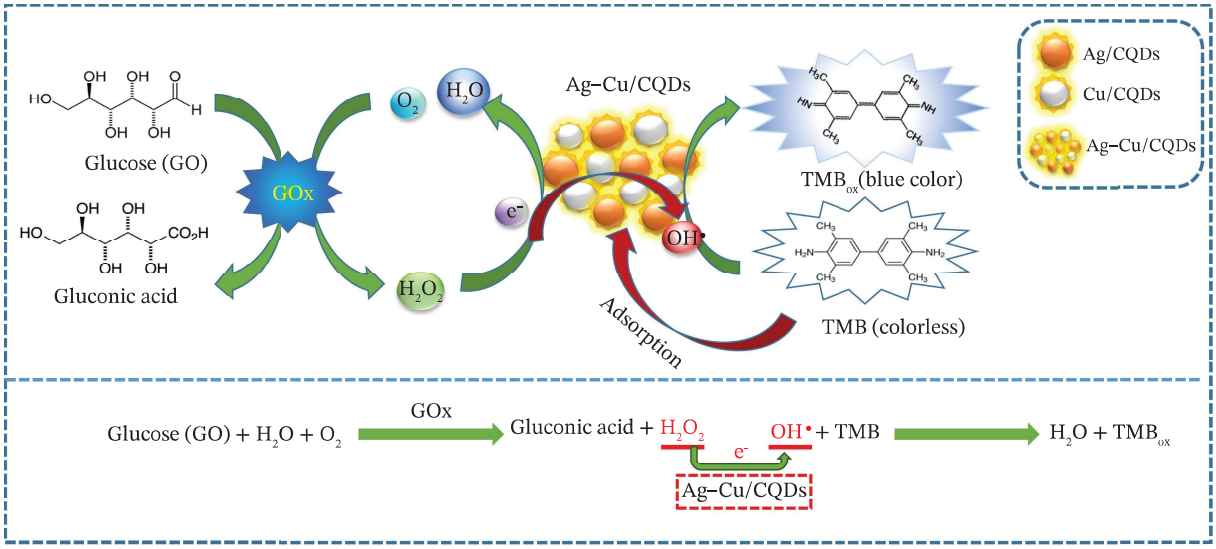

SCHEME 2 | The proposed mechanism for GL detection by colorimetric method based on Ag–Cu/CQDs.

TABLE 3 | Determination of GL in human urine samples.

Samples	Added (μM)	Found (μM)	Average (μM)	Recovery (%)	RSD (%) ($n = 3$)
Blank	—	0	—	—	—
S1	1800	1860.5 1837.3 1845.2	1847.7	102.6	0.64
S2	1600	1568.4 1637.2 1595.4	1600.4	100.0	2.17
S3	1000	1058.1 1034.7 1036.7	1043.2	104.3	1.24

under the optimized conditions. These results confirm that the colorimetric method developed from Ag–Cu/CQDs materials has the potential for effective application in GL detection in real biological samples.

4 | Conclusion

This study successfully synthesized Ag–Cu/CQDs materials with tight binding between AgNPs and CuNPs on CQDs. CQDs were synthesized by a green method from TS, acting as both a reducing agent and a stabilizing agent, helping to reduce Ag^+ and Cu^{2+} ions into corresponding metal nanoparticles. The synthesized materials showed excellent peroxidase-mimicking activity, which could combine with H_2O_2 to produce $OH^•$ and oxidize colorless TMB into characteristic blue TMB_{ox}. Based on this principle, we developed a simple, sensitive, and selective colorimetric method for the detection of GL by coupling with GOx, in which Ag–Cu/CQDs acted as a peroxidase-mimicking catalyst. The detection system achieved LODs of 0.14 and 0.06 mM for H_2O_2 and GL, respectively, and was successfully applied to the analysis of urine samples with high recoveries. Compared with natural peroxidase enzymes, Ag–Cu/CQDs have outstanding advantages such as a simple synthesis process, high stability, and low cost. In addition, this study also elucidated the catalytic mechanism of Ag–Cu/CQDs in the peroxidase-mimicking reaction, which provides a scientific basis for optimizing GL detection performance in future biomedical and environmental applications.

Funding

No funding was received for this manuscript.

Ethics Statement

This study was approved by the Biomedical Research Ethics Committee of Duy Tan University (Application No. DTU/REC2025/NHH17). Informed consent was obtained from all subjects participating in this study.

Conflicts of Interest

The authors declare no conflicts of interest.

Data Availability Statement

The authors confirm that the data supporting the findings are available within the article.

References

1. N. H. Cho, J. Shaw, S. Karuranga, et al., "IDF Diabetes Atlas: Global Estimates of Diabetes Prevalence for 2017 and Projections for 2045," *Diabetes Research and Clinical Practice* 138 (2018): 271–281, https://doi.org/10.1016/j.diabres.2018.02.023.

2. H. Lee, Y. J. Hong, S. Baik, T. Hyeon, and D. H. Kim, "Enzyme-Based Glucose Sensor: From Invasive to Wearable Device," *Advanced Healthcare Materials* 1701150, no. 8 (2018): 1–14, https://doi.org/10.1002/adhm.201701150.

3. Y. Song, K. Qu, C. Zhao, J. Ren, and X. Qu, "Graphene Oxide: Intrinsic Peroxidase Catalytic Activity and Its Application to Glucose Detection," *Advanced Materials* 22, no. 19 (2010): 2206–2210, https://doi.org/10.1002/adma.200903783.

4. S. Jiang, Y. Zhang, Y. Yang, et al., "Glucose Oxidase-Instructed Fluorescence Amplification Strategy for Intracellular Glucose Detection," *ACS Applied Materials and Interfaces* 11, no. 11 (2019): 10554–10558, https://doi.org/10.1021/acsami.9b00010.

5. Y. Duan, Y. Huang, S. Chen, W. Zuo, and B. Shi, "Cu-Doped Carbon Dots as Catalysts for the Chemiluminescence Detection of Glucose," *ACS Omega* 4, no. 6 (2019): 9911–9917, https://doi.org/10.1021/acsomega.9b00738.

6. Y. Zhang, J. Xu, J. Xia, F. Zhang, and Z. Wang, "MOF-Derived Porous Ni2P/Graphene Composites With Enhanced Electrochemical Properties for Sensitive Nonenzymatic Glucose Sensing," *ACS Applied Materials and Interfaces* 10, no. 45 (2018): 39151–39160, https://doi.org/10.1021/acsami.8b11867.

7. W. Liu, J. Tian, C. Mao, et al., "Sulfur Vacancy Promoted Peroxidase-Like Activity of Magnetic Greigite (Fe3S4) for Colorimetric Detection of Serum Glucose," *Analytica Chimica Acta* 1127 (2020): 246–255, https://doi.org/10.1016/j.aca.2020.06.056.

8. C. Lu, X. Liu, Y. Li, et al., "Multifunctional Janus Hematite-Silica Nanoparticles: Mimicking Peroxidase-Like Activity and Sensitive Colorimetric Detection of Glucose," *ACS Applied Materials and Interfaces* 7, no. 28 (2015): 15395–15402, https://doi.org/10.1021/acsami.5b03423.

9. H. Wei and E. Wang, "Fe3O4 Magnetic Nanoparticles as Peroxidase Mimetics and Their Applications in H2O2 and Glucose Detection," *Analytical Chemistry* 80, no. 6 (2008): 2250–2254, https://doi.org/10.1021/ac702203f.

10. Z. Yang, Y. Cao, J. Li, M. Lu, Z. Jiang, and X. Hu, "Smart CuS Nanoparticles as Peroxidase Mimetics for the Design of Novel Label-Free Chemiluminescent Immunoassay," *ACS Applied Materials and Interfaces* 8, no. 19 (2016): 12031–12038, https://doi.org/10.1021/acsami.6b02481.

11. H. V. Tran, N. D. Nguyen, A. T. Le, L. T. Tran, T. D. Le, and C. D. Huynh, "Fe3O4@C Magnetite Nanocomposite: An Artificial Peroxidase Nanozyme for the Development of a Colorimetric Glucose Biosensor," *New Journal of Chemistry* 48, no. 47 (2024): 20007–20017, https://doi.org/10.1039/d4nj03808h.

12. J. Yu, T. Chen, X. Wen, H. Shi, L. Wang, and Y. Xu, "Highly Selective Nanozyme-Based Glucose Sensing Platform via Construction of Artificial Recognition Sites on Gold Nanospheres," *Biosensors and Bioelectronics* 253 (2024): 116169, https://doi.org/10.1016/j.bios.2024.116169.

13. C. Cirillo, M. Iuliano, and M. Sarno, "ZnFe2O4/GQDs Nanoparticles as Peroxidase Mimics for Sensitive and Selective Colorimetric Detection of Glucose in Real Samples," *Micromachines* 16, no. 5 (2025): 520, https://doi.org/10.3390/mi16050520.

14. S. Bin He, A. Hu, Q. Zhuang, et al., "Ascorbate Oxidase Mimetic Activity of Copper(II) Oxide Nanoparticles," *ChemBioChem* 21, no. 7 (2020): 978–984, https://doi.org/10.1002/cbic.201900595.

15. J. Mu, Y. Wang, M. Zhao, and L. Zhang, "Intrinsic Peroxidase-Like Activity and Catalase-Like Activity of Co3O4 Nanoparticles," *Chemical Communications* 48, no. 19 (2012): 2540–2542, https://doi.org/10.1039/c2cc17013b.

16. Y. Song, W. Wei, and X. Qu, "Colorimetric Biosensing Using Smart Materials," *Advanced Materials* 23, no. 37 (2011): 4215–4236, https://doi.org/10.1002/adma.201101853.

17. J. Xie, X. Zhang, H. Wang, H. Zheng, Y. Huang, and J. Xie, "Analytical and Environmental Applications of Nanoparticles as Enzyme Mimetics," *TrAC, Trends in Analytical Chemistry* 39 (2012): 114–129, https://doi.org/10.1016/j.trac.2012.03.021.

18. J. L. Ma, B. C. Yin, X. Wu, and B. C. Ye, "Simple and Cost-Effective Glucose Detection Based on Carbon Nanodots Supported on Silver Nanoparticles," *Analytical Chemistry* 89, no. 2 (2017): 1323–1328, https://doi.org/10.1021/acs.analchem.6b04259.

19. A. Koyappayil, S. Berchmans, and M. H. Lee, "Dual Enzyme-Like Properties of Silver Nanoparticles Decorated Ag2WO4 Nanorods and Its Application for H2O2 and Glucose Sensing," *Colloids and Surfaces, B: Biointerfaces* 189, no. January (2020): 110840, https://doi.org/10.1016/j.colsurfb.2020.110840.

20. P. H. Hsiao and C. Y. Chen, "Insights for Realizing Ultrasensitive Colorimetric Detection of Glucose Based on Carbon/Silver Core/Shell Nanodots," *ACS Applied Bio Materials* 2, no. 6 (2019): 2528–2538, https://doi.org/10.1021/acsabm.9b00228.

21. L. Han, C. Li, T. Zhang, Q. Lang, and A. Liu, "Au@Ag Heterogeneous Nanorods as Nanozyme Interfaces With Peroxidase-Like Activity and Their Application for One-Pot Analysis of Glucose at Nearly Neutral pH," *ACS Applied Materials and Interfaces* 7, no. 26 (2015): 14463–14470, https://doi.org/10.1021/acsami.5b03591.

22. Y. H. Won and L. A. Stanciu, "Cu2O and Au/Cu2O Particles: Surface Properties and Applications in Glucose Sensing," *Sensors (Switzerland)* 12, no. 10 (2012): 13019–13033, https://doi.org/10.3390/s121013019.

23. C. Jiang, X. Wei, S. Bao, H. Tu, and W. Wang, "Cu@Au(Ag)/Pt Nanocomposite as Peroxidase Mimic and Application of Cu@Au/Pt in Colorimetric Detection of Glucose and l-Cysteine," *RSC Advances* 9, no. 71 (2019): 41561–41568, https://doi.org/10.1039/c9ra08547e.

24. S. Si and T. K. Mandal, "Tryptophan-Based Peptides to Synthesize Gold and Silver Nanoparticles: A Mechanistic and Kinetic Study," *Chemistry–A European Journal* 13, no. 11 (2007): 3160–3168, https://doi.org/10.1002/chem.200601492.

25. H. H. Jing, F. Bardakci, S. Akgöl, et al., "Green Carbon Dots: Synthesis, Characterization, Properties and Biomedical Applications," *Journal of Functional Biomaterials* 14, no. 1 (2023): 27, https://doi.org/10.3390/jfb14010027.

26. R. Atchudan, T. N. Jebakumar Immanuel Edison, M. Shanmugam, S. Perumal, T. Somanathan, and Y. R. Lee, "Sustainable Synthesis of Carbon Quantum Dots From Banana Peel Waste Using Hydrothermal Process for in Vivo Bioimaging," *Physica E: Low-dimensional Systems and Nanostructures* 126, no. September 2020 (2021): 114417, https://doi.org/10.1016/j.physe.2020.114417.

27. N. Dhenadhayalan, K. C. Lin, and T. A. Saleh, "Recent Advances in Functionalized Carbon Dots Toward the Design of Efficient Materials for Sensing and Catalysis Applications," *Small* 16, no. 1 (2020): 1–24, https://doi.org/10.1002/smll.201905767.

28. M. Choppadandi, A. T. Guduru, P. Gondaliya, et al., "Structural Features Regulated Photoluminescence Intensity and Cell Internalization of Carbon and Graphene Quantum Dots for Bioimaging," *Materials Science and Engineering: C* 129, no. August (2021): 112366, https://doi.org/10.1016/j.msec.2021.112366.

29. Y. Chen, C. Yang, X. Huang, et al., "Two-Dimensional MXene Enabled Carbon Quantum Dots@Ag With Enhanced Catalytic Activity Towards the Reduction of p-Nitrophenol," *RSC Advances* 12, no. 8 (2022): 4836–4842, https://doi.org/10.1039/d1ra09177h.

30. Y. Han, H. Huang, H. Zhang, et al., "Carbon Quantum Dots With Photoenhanced Hydrogen-Bond Catalytic Activity in Aldol Condensations," *ACS Catalysis* 4, no. 3 (2014): 781–787, https://doi.org/10.1021/cs401118x.

31. D. Bruen, C. Delaney, L. Florea, and D. Diamond, "Glucose Sensing for Diabetes Monitoring: Recent Developments," *Sensors (Switzerland)* 17, no. 8 (2017): 1–21, https://doi.org/10.3390/s17081866.

32. N. K. Khairol Anuar, H. L. Tan, Y. P. Lim, M. S. So'aib, and N. F. Abu Bakar, "A Review on Multifunctional Carbon-Dots Synthesized From Biomass Waste: Design/Fabrication, Characterization and Applications," *Frontiers in Energy Research* 9, no. April (2021): 1–22, https://doi.org/10.3389/fenrg.2021.626549.

33. H. N. Q, H. T. ThiHoaLe, Ta Thi NgocAnh, N. Thi ThuHuong, and Le T. T. Nhi, *Green Catalysts AuNPs/CQDs From Turmeric Starch: An Effective Solution in 4-Nitrophenol Reduction* (IOPscience, 2025).

34. X. Zhang, X. Liu, Z. Lin, et al., "Colorimetric/Fluorescence Dual-Mode Sensor Based on Acid Phosphatase/Peroxidase-Mimicking Cascade Catalysis for Ultrasensitive Detection of Tartaric Acid," *Microchemical Journal* 213 (2025): 113850, https://doi.org/10.1016/j.microc.2025.113850.

35. Y. Dong, Z. Yang, Q. Sheng, and J. Zheng, "Solvothermal Synthesis of Ag@Fe3O4 Nanosphere and Its Application as Hydrazine Sensor," *Colloids and Surfaces A: Physicochemical and Engineering Aspect* 538 (2018): 371–377, https://doi.org/10.1016/j.colsurfa.2017.11.024.

36. W. J. Aziz and H. A. Jassim, "A New Paradigm Shift to Prepare Copper Nanoparticles Using Biological Synthesis and Evaluation of Antimicrobialactivity," *Plant Archives* 18, no. 2 (2018): 2020–2024.

37. M. Karimzadeh, K. Niknam, N. Manouchehri, and D. Tarokh, "A Green Route for the Cross-Coupling of Azide Anions With Aryl Halides Under Both Base and Ligand-Free Conditions: Exceptional Performance of a Cu2O-CuO-Cu-C Nanocomposite," *RSC Advances* 8, no. 45 (2018): 25785–25793, https://doi.org/10.1039/c8ra04608e.

38. H. T. Nguyen, T. T. N. Le, M. T. Truong, et al., "Au/Ag2MoO4 Nanocomposite: A Dual-Function Catalyst for Dye Degradation and Colorimetric Detection," *Materials Today Communications* 39, no. October 2023 (2024): 108831, https://doi.org/10.1016/j.mtcomm.2024.108831.

39. A. Kechagias, C. Lykos, V. K. Karabagias, et al., "Development and Characterization of N/S-Carbon Quantum Dots by Valorizing Greek Crayfish Food Waste," *Applied Sciences* 13, no. 15 (2023): 8730, https://doi.org/10.3390/app13158730.

40. V. Manikandan and N. Y. Lee, "Green Synthesis of Carbon Quantum Dots and Their Environmental Applications," *Environmental Research* 212, no. PB (2022): 113283, https://doi.org/10.1016/j.envres.2022.113283.

41. Y. Li, M. Qiu, P. Guo, et al., "Core-Shell Structure N-Doped Graphene Quantum Dots Fe3O4/Co3O4 Nanoparticles for Colorimetric Detection of H2O2," *Colloids and Surfaces A: Physicochemical and Engineering Aspect* 693, no. January (2024): 134061, https://doi.org/10.1016/j.colsurfa.2024.134061.

42. S. Ghosh, S. S. Satapathy, K. Ghosh, S. Jauhari, S. K. Panda, and S. Si, "Carbon Dots Assisted Synthesis of Gold Nanoparticles and Their Catalytic Activity in 4-Nitrophenol Reduction," *ChemistrySelect* 4, no. 12 (2019): 3416–3422, https://doi.org/10.1002/slct.201804040.

43. H. Sun, X. Liu, X. Wang, et al., "Colorimetric Determination of Ascorbic Acid Using a Polyallylamine-Stabilized IrO2/Graphene Oxide Nanozyme as a Peroxidase Mimic," *Microchimica Acta* 187, no. 2 (2020): https://doi.org/10.1007/s00604-019-3897-4.

44. D. Yang, J. Liu, W. Hu, et al., "Nano-Ferroelectric Oxidase Mimics for Colorimetric Detection of Glutathione," *Sensors and Actuators, B: Chemical* 393, no. June (2023): 134170, https://doi.org/10.1016/j.snb.2023.134170.

45. Z. Xin, K. Duan, Q. Zhuo, et al., "Novel Nanozyme Ag/Fe3O4@h-BN With Peroxidase-Mimicking and Oxidase-Mimicking Activities for Dye Degradation, As(V) Removal and Detection," *Chemical Engineering Journal* 461, no. January (2023): 141589, https://doi.org/10.1016/j.cej.2023.141589.

46. A. Abbasnia, A. Zarei, M. Yeganeh, H. R. Sobhi, M. Gholami, and A. Esrafili, "Removal of Tetracycline Antibiotics by Adsorption and Photocatalytic-Degradation Processes in Aqueous Solutions Using Metal Organic Frameworks (MOFs): A Systematic Review," *Inorganic Chemistry Communications* 145, no. May (2022): 109959, https://doi.org/10.1016/j.inoche.2022.109959.

47. P. P.D. McGinness and J. Kirkpatrick, "A Superoxide-Producing System in the Conjuctival Mucus Thread," *Investigative Ophthalmology & Visual Science* (1977).

48. V. C. N. Anh, L. T. T. Nhi, L. T. K. Dung, et al., "Photocatalytic Degradation of Methylene Blue Under Visible Light by Cobalt Ferrite Nanoparticles/Graphene Quantum Dots," *Beilstein Journal of Nanotechnology* 15 (2024): 475–489, https://doi.org/10.3762/BJNANO.15.43.

49. W. Tan, G. Yao, H. Yu, et al., "Ultra-Trace Ag Doped Carbon Quantum Dots With Peroxidase-Like Activity for the Colorimetric Detection of Glucose," *Food Chemistry* 447, no. February (2024): 139020, https://doi.org/10.1016/j.foodchem.2024.139020.

50. S. A. Geleto, A. M. Ariti, B. T. Gutema, et al., "Nanocellulose/Fe3O4/Ag Nanozyme With Robust Peroxidase Activity for Enhanced Antibacterial and Wound Healing Applications," *ACS Omega* 8, no. 51 (2023): 48764–48774, https://doi.org/10.1021/acsomega.3c05748.

51. D. Bano, V. Kumar, V. K. Singh, et al., "A Facile and Simple Strategy for the Synthesis of Label Free Carbon Quantum Dots From the Latex of Euphorbia milii and Its Peroxidase-Mimic Activity for the Naked Eye Detection of Glutathione in a Human Blood Serum," *ACS Sustainable Chemistry & Engineering* 7, no. 2 (2019): 1923–1932, https://doi.org/10.1021/acssuschemeng.8b04067.

52. L. Su, J. Feng, X. Zhou, C. Ren, H. Li, and X. Chen, "Colorimetric Detection of Urine Glucose Based ZnFe2O4 Magnetic Nanoparticles," *Analytical Chemistry* 84, no. 13 (2012): 5753–5758, https://doi.org/10.1021/ac300939z.

53. T. Pirmohamed, J. M. Dowding, S. Singh, et al., "Nanoceria Exhibit Redox State-Dependent Catalase Mimetic Activity," *Chemical Communications* 46, no. 16 (2010): 2736–2738, https://doi.org/10.1039/b922024k.

54. Z. Wang, M. Chen, J. Shu, and Y. Li, "One-Step Solvothermal Synthesis of Fe3O4@Cu@Cu2O Nanocomposite as Magnetically Recyclable Mimetic Peroxidase," *Journal of Alloys and Compounds* 682 (2016): 432–440, https://doi.org/10.1016/j.jallcom.2016.04.269.

55. Y. Liu and F. Yu, "Substrate-Specific Modifications on Magnetic Iron Oxide Nanoparticles as an Artificial Peroxidase for Improving Sensitivity in Glucose Detection," *Nanotechnology* 22, no. 14 (2011): 145704, https://doi.org/10.1088/0957-4484/22/14/145704.

56. L. Gao, J. Zhuang, L. Nie, et al., "Intrinsic Peroxidase-Like Activity of Ferromagnetic Nanoparticles," *Nature Nanotechnology* 2, no. 9 (2007): 577–583, https://doi.org/10.1038/nnano.2007.260.

57. N. R. N. Vinita and R. Prakash, "One Step Synthesis of AuNPs@MoS2-QDs Composite as a Robust Peroxidase-Mimetic for Instant Unaided Eye Detection of Glucose in Serum, Saliva and Tear," *Sensors and Actuators, B: Chemical* 263, no. February (2018): 109–119, https://doi.org/10.1016/j.snb.2018.02.085.

58. Q. Zeng, M. Xu, W. Hu, et al., "Porous Colorimetric Microneedles for Minimally Invasive Rapid Glucose Sampling and Sensing in Skin Interstitial Fluid," *Biosensors* 13, no. 5 (2023): 1–13, https://doi.org/10.3390/bios13050537.

59. Y. Guo, H. Wang, X. Ma, et al., "Fabrication of Ag-Cu2O/Reduced Graphene Oxide Nanocomposites as Surface-Enhanced Raman Scattering Substrates for in Situ Monitoring of Peroxidase-Like Catalytic Reaction and Biosensing," *ACS Applied Materials and Interfaces* 9, no. 22 (2017): 19074–19081, https://doi.org/10.1021/acsami.7b02149.

60. C. Jiang, J. Zhu, Z. Li, J. Luo, J. Wang, and Y. Sun, "Chitosan–Gold Nanoparticles as Peroxidase Mimic and Their Application in Glucose Detection in Serum," *RSC Advances* 7, no. 70 (2017): 44463–44469, https://doi.org/10.1039/C7RA08967H.

61. T. Peik-See, A. Pandikumar, L. H. Ngee, H. N. Ming, and C. C. Hua, "Magnetically Separable Reduced Graphene Oxide/Iron Oxide Nanocomposite Materials for Environmental Remediation," *Catalysis Science and Technology* 4, no. 12 (2014): 4396–4405, https://doi.org/10.1039/c4cy00806e.

62. G. Lee, C. Kim, D. Kim, et al., "Multibranched au-ag-pt Nanoparticle as a Nanozyme for the Colorimetric Assay of Hydrogen Peroxide and Glucose," *ACS Omega* 7, no. 45 (2022): 40973–40982, https://doi.org/10.1021/acsomega.2c04129.

63. B. Xu, X. Xiang, Z. Ding, Z. Luo, and J. Huang, "A Colorimetric Assay for Detection of Glucose by Enzymatic Etching of Triangular Gold Nanosheets," *Materials Chemistry and Physics* 301, no. March (2023): 127619, https://doi.org/10.1016/j.matchemphys.2023.127619.

64. Y. Guo, L. Yan, R. Zhang, H. Ren, and A. Liu, "CoO-Supported Ordered Mesoporous Carbon Nanocomposite Based Nanozyme With Peroxidase-Like Activity for Colorimetric Detection of Glucose," *Process Biochemistry* 81 (2019): 92–98, https://doi.org/10.1016/j.procbio.2019.03.005.

65. A. Dager, T. Uchida, T. Maekawa, and M. Tachibana, "Synthesis and Characterization of Mono-Disperse Carbon Quantum Dots From Fennel Seeds: Photoluminescence Analysis Using Machine Learning," *Scientific Reports* 9, no. 1 (2019): 1–10, https://doi.org/10.1038/s41598-019-50397-5.

66. K. Mitra, A. B. Ghosh, A. Sarkar, N. Saha, and A. K. Dutta, "Colorimetric Estimation of Human Glucose Level Using γ-Fe 2O3 Nanoparticles: An Easily Recoverable Effective Mimic Peroxidase," *Biochemical and Biophysical Research Communications* 451, no. 1 (2014): 30–35, https://doi.org/10.1016/j.bbrc.2014.07.028.

67. S. Cai, Q. Han, C. Qi, et al., "Pt74Ag26 Nanoparticle-Decorated Ultrathin MoS2 Nanosheets as Novel Peroxidase Mimics for Highly Selective Colorimetric Detection of H2O2 and Glucose," *Nanoscale* 8, no. 6 (2016): 3685–3693, https://doi.org/10.1039/c5nr08038j.

68. W. Qin, H. Tian, Z. Meng, Z. Tang, J. Wang, and Z. Wu, "Facile Synthesis and Ozonation of Carbon Dots Using Mango Pulps for Dual-Mode Colorimetry and Ratiometric Fluorescence Detection of Sarcosine," *Microchemical Journal* 195, no. October (2023): 109468, https://doi.org/10.1016/j.microc.2023.109468.

69. Y. Wang and A. Hu, "Carbon Quantum Dots: Synthesis, Properties and Applications," *Journal of Materials Chemistry C* 2, no. 34 (2014): 6921–6939, https://doi.org/10.1039/c4tc00988f.

70. N. A. A. Nazri, N. H. Azeman, Y. Luo, and A. A. A. Bakar, "Carbon Quantum Dots for Optical Sensor Applications: A Review," *Optics and Laser Technology* 139, no. January (2021): 106928, https://doi.org/10.1016/j.optlastec.2021.106928.

71. X. Liu, D. Huang, C. Lai, et al., "Peroxidase-Like Activity of Smart Nanomaterials and Their Advanced Application in Colorimetric Glucose Biosensors," *Small* 15, no. 17 (2019): 1–27, https://doi.org/10.1002/smll.201900133.

72. X. Zhang, H. Zhao, Y. Xue, et al., "Colorimetric Sensing of Clenbuterol Using Gold Nanoparticles in the Presence of Melamine," *Biosensors and Bioelectronics* 34, no. 1 (2012): 112–117, https://doi.org/10.1016/j.bios.2012.01.026.